# RSC Advances

This is an *Accepted Manuscript*, which has been through the Royal Society of Chemistry peer review process and has been accepted for publication.

*Accepted Manuscripts* are published online shortly after acceptance, before technical editing, formatting and proof reading. Using this free service, authors can make their results available to the community, in citable form, before we publish the edited article. This *Accepted Manuscript* will be replaced by the edited, formatted and paginated article as soon as this is available.

You can find more information about *Accepted Manuscripts* in the **Information for Authors**.

ROYAL SOCIETY OF CHEMISTRY

www.rsc.org/advances

# *Phase Diagram for Nano Yttria-Stabilized Zirconia System*

*Mohammad Asadikiya [a,b], Hooman Sabarou [a,b], Ming Chen [c], Yu Zhong [a,b]*

[a] *Department of Mechanical and Materials Engineering, Florida International University, Miami, Florida 33174, USA*
[b] *Center for the Study of Matter at Extreme Conditions (CeSMEC), Florida International University, Miami, Florida 33199, USA*
[c] *Department of Energy Conversion and Storage, Technical University of Denmark, DK-4000 Roskilde, Denmark*

## *Abstract:*

Due to attractive properties of nano particles because of their effective surface area, they have been studied widely. Nano yttria-stabilized zirconia (n-YSZ) is a ceramic, which has been scrutinized extensively during past years. Because of different stability behavior of n-YSZ in comparison with bulk YSZ, a new phase diagram is needed for n-YSZ system in order to identify stable phases in various conditions. In this study, a phase diagram for n-YSZ system was provided to determine phase stability ranges at room temperature with respect to particle size and composition. The CALPHAD approach was applied to calculate the Gibbs energy of bulk YSZ. It was combined with the surface energy of each phase in n-YSZ system i.e. monoclinic, tetragonal, cubic, and amorphous to produce the total Gibbs energy of each individual phase of n-YSZ system. By applying the CALPHAD approach, a 3-D phase diagram for n-YSZ system was established in which the stability range of each individual phase can be predicted based on the particle size, composition, and temperature.

## 1. *Introduction:*

Yttria-stabilized zirconia (YSZ) is one of the most interesting ceramic systems which has been studied extensively because of its critical applications. Tetragonal polymorph is used as advanced structural ceramic like tooth crowns and jet engines since it has high toughness [1][2][3]. Cubic polymorph has the ability of conducting oxygen ions due to the high oxygen vacancy concentration, which increases when temperature rises [3]. This characteristic of cubic polymorph is the reason of its applicability in solid oxide fuel cells (SOFCs) and oxygen sensors [4][5][6]. Figure 1 shows the crystal structure of YSZ polymorphs.
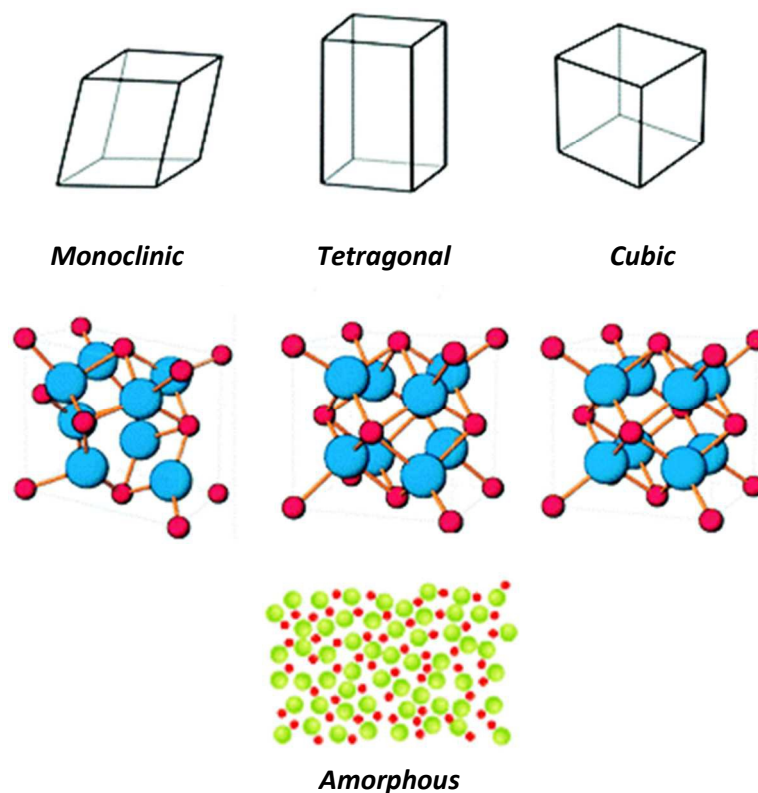
*Figure 1- Crystal structures of YSZ polymorphs.*

Nano crystalline YSZ (n-YSZ) has been investigated recently because of its different properties with respect to the bulk. For example, one important factor in the gas sensors is response time which is related to electrode microstructure because of the effect of surface diffusion. Particles with smaller grain size and higher specific surface help reducing the response time. The larger surface area also causes higher catalytic activities [7]. n-YSZ properties are attributed to the large fraction of atoms within the interface region [8]. In fact, in the systems with nano sized particles, the effect of surface area becomes significant and affects the Gibbs energy of each phase [9][10]. Therefore, n-YSZ system shows different behavior in comparison with the bulk YSZ. In other words, the stability regions in n-YSZ system can be significantly different from that of the bulk YSZ.

For the bulk YSZ system, different groups have conducted extensive studies to understand the phase regions at different temperatures and compositions [11][12][13][14]. However, for n-YSZ system, there is no applicable accurate phase diagram especially at elevated temperatures.

In this study, the CALPHAD (Calculation of Phase Diagrams) approach was applied to predict the Gibbs energy of bulk YSZ system. By considering the effect of surface energy, the total Gibbs energy of n-YSZ system was developed. Therefore, by predicting the total Gibbs energy of each polymorph in a range of temperature, a 3-D phase diagram for n-YSZ system was established in which the stability range of each crystal structure can be determined based on the particle size, composition, and temperature.

## 2. Background review:

Several groups have attempted to observe the changes in the transformation temperatures as a function of grain size for n-YSZ system [2][3][15][16]. The total surface energy is consisting of surface area and specific surface energy. Hence, to have Gibbs energy definition for n-YSZ system, the specific surface energy has to be measured. Based on the recent advancements in microcalorimetry for measuring specific surface energy of nano particles, Drazin and Castro have measured multiple specific surface energies in the n-YSZ system for yttria mole fraction of 0 to 0.2 at room temperature [17]. Water adsorption microcalorimetry theory was applied to collect the specific surface energy data [18]. The experiments were done for m-$ZrO_2$, t-$ZrO_2$, c-$ZrO_2$, and liquid phases with the particle size of 32.4 to 39.8 nm, 14.2 to 17.7 nm, 4 to 6.3 nm, and 1 to 1.1 nm respectively.

## 3. Thermodynamic Modeling:

### 3.1. Gibbs energy calculation for the bulk materials:

The CALPHAD approach relies on modeling the Gibbs energies of each individual phases in the system. This characteristic state function is of particular interest because the Gibbs energy is minimized at equilibrium under constant temperature and pressure. Temperature and pressure are the variables that are typically controlled experimentally. The thermodynamic databases based on the Gibbs energies are then constructed using experimental data and programs like Thermo-Calc [19].

The thermodynamic database for the $ZrO_2$-$Y_2O_3$ system was provided by Chen et al. [13]. It was applied in the current study to calculate the Gibbs energy of each phase for the

bulk YSZ at different temperatures. Equation below is for the Gibbs free energy of bulk materials:

$$\Delta G_{bulk} = \Delta H - T\Delta S \qquad (1)$$

in which H is enthalpy, T is temperature and S is entropy.

The model used for m-ZrO$_2$ (monoclinic YSZ phase) and t-ZrO$_2$ (tetragonal YSZ phase) in the database by Chen et al. is $(Y^{3+},Zr^{4+})_1(O^{2-},Va)_2$ [13]. In this model, the first sublattice is occupied by Y$^{3+}$ and Zr$^{4+}$ ions and the second one is occupied by O$^{2-}$ ion and vacancy. The model used for c-ZrO$_2$ (cubic YSZ phase) is $(Y,Y^{3+},Zr,Zr^{4+})_1(O^{2-},Va)_2$. Thus, the Gibbs energy of the m-ZrO$_2$ and t-ZrO$_2$ phases are given by:

$G_m = y_{Y^{3+}} y_{O^{2-}} \,{}^{\circ}G_{Y^{3+}:O^{2-}} + y_{Zr^{4+}} y_{O^{2-}} \,{}^{\circ}G_{Zr^{4+}:O^{2-}} + y_{Y^{3+}} y_{Va} \,{}^{\circ}G_{Y^{3+}:Va} + y_{Zr^{4+}} y_{Va} \,{}^{\circ}G_{Zr^{4+}:Va} + RT[y_{Y^{3+}} \ln y_{Y^{3+}} + y_{Zr^{4+}} \ln y_{Zr^{4+}} + 2(y_{O^{2-}} \ln y_{O^{2-}} + y_{Va} \ln y_{Va})] + {}^E G_m$

And the Gibbs energy of the c-ZrO$_2$ phase is given by:

$G'_m = y_{Y^{3+}} y_{O^{2-}} \,{}^{\circ}G_{Y^{3+}:O^{2-}} + y_{Zr^{4+}} y_{O^{2-}} \,{}^{\circ}G_{Zr^{4+}:O^{2-}} + y_{Y^{3+}} y_{Va} \,{}^{\circ}G_{Y^{3+}:Va} + y_{Zr^{4+}} y_{Va} \,{}^{\circ}G_{Zr^{4+}:Va} + y_Y y_{O^{2-}} \,{}^{\circ}G_{Y:O^{2-}} + y_{Zr} y_{O^{2-}} \,{}^{\circ}G_{Zr:O^{2-}} + y_Y y_{Va} \,{}^{\circ}G_{Y:Va} + y_{Zr} y_{Va} \,{}^{\circ}G_{Zr:Va} + RT[y_Y \ln y_Y + y_{Y^{3+}} \ln y_{Y^{3+}} + y_{Zr} \ln y_{Zr} + y_{Zr^{4+}} \ln y_{Zr^{4+}} + 2(y_{O^{2-}} \ln y_{O^{2-}} + y_{Va} \ln y_{Va})] + {}^E G'_m$

where $y_j$ is site fraction of specie j in a particular sublattice. The excess Gibbs energy ${}^E G_m$ is defined as below:

${}^E G_m = y_{Y^{3+}} y_{Zr^{4+}} y_{O^{2-}} \sum_{i=0}^{n} {}^{i}L_{Y^{3+},Zr^{4+}:O^{2-}} (y_{Y^{3+}} - y_{Zr^{4+}})^i + y_{Y^{3+}} y_{Zr^{4+}} y_{Va} \sum_{i=0}^{n} {}^{i}L_{Y^{3+},Zr^{4+}:Va} (y_{Y^{3+}} - y_{Zr^{4+}})^i$

And the excess Gibbs energy ${}^E G'_m$ is defined as below:

${}^E G'_m = y_{Y^{3+}} y_{Zr^{4+}} y_{O^{2-}} \sum_{i=0}^{n} {}^{i}L_{Y^{3+},Zr^{4+}:O^{2-}} (y_{Y^{3+}} - y_{Zr^{4+}})^i + y_{Y^{3+}} y_{Zr^{4+}} y_{Va} \sum_{i=0}^{n} {}^{i}L_{Y^{3+},Zr^{4+}:Va} (y_{Y^{3+}} - y_{Zr^{4+}})^i + y_{Zr} y_{Zr^{4+}} y_{O^{2-}} \sum_{i=0}^{n} {}^{i}L_{Zr,Zr^{4+}:O^{2-}} (y_{Zr} - y_{Zr^{4+}})^i + y_{Zr} y_{Zr^{4+}} y_{Va} \sum_{i=0}^{n} {}^{i}L_{Zr,Zr^{4+}:Va} (y_{Zr} - y_{Zr^{4+}})^i$

where ${}^iL$ is the interaction parameter with the form of A+BT. If i=0, the solution is regular, if i=1, the solution is sub-regular, and if i=2, the solution is sub-sub-regular.

The interaction parameter for m-ZrO$_2$ phase was considered zero since yttria concentration in m-ZrO$_2$ is extremely low and it is proper to be treated as an ideal solution. t-ZrO$_2$ phase was considered as a regular solution and c-ZrO$_2$ was treated as a sub-regular solution in the database by Chen et al. [13].

### 3.2. *T-zero temperature method to determine phase boundaries:*

In order to calculate the Gibbs energy for bulk YSZ, partial equilibria simulation has been applied. Since the kinetics is very slow in the YSZ system, phase transitions are observed with a considerable delay. The m-ZrO$_2$↔t-ZrO$_2$ transition occurs as a

martensitic transformation [13]. In order to determine the phase boundaries under such conditions, Kaufman and Cohen suggested T-zero temperature approach [20], which is one type of the partial equilibrium method. In this method, the starting transition temperature of tetragonal to monoclinic phases during cooling and also the starting transition temperature of monoclinic to tetragonal phases during heating are captured. Based on these two transition temperatures, an average temperature is calculated as the equilibrium temperature. In other words, $T_0$ is a temperature in which the Gibbs energies of two adjacent phases are equal in a determined composition. $T_0$ temperature is located in the two-phase region and it is a theoretical limit for a diffusionless transformation as illustrated in Figure 2. In this figure, $u_j$ is defined as the site fraction of element j with reference to the substitutional sublattices only.
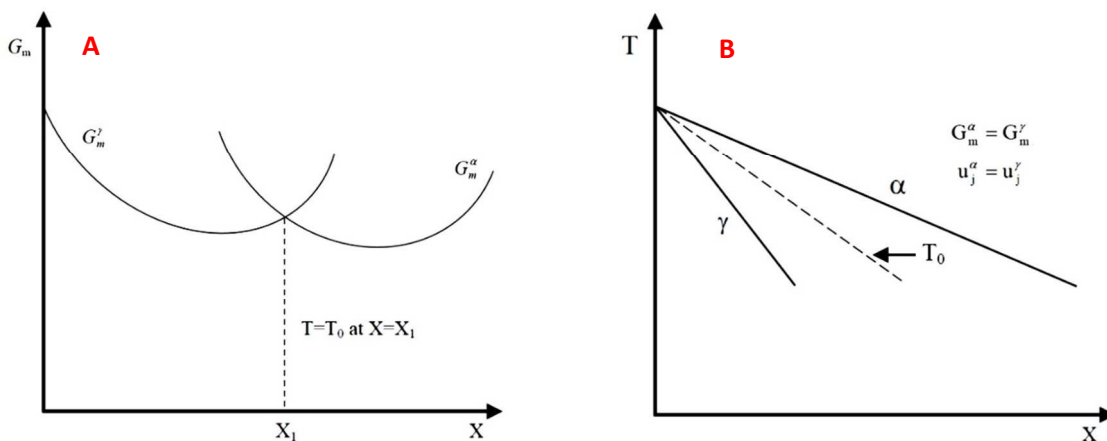


*Figure 2- T-zero temperature method. A) To temperature as a point at a defined composition, B) To temperature as a line when the composition changes.*

### 3.3.   *Amorphous phase modeling:*

The model for ionic liquid was used to calculate the amorphous phase. In the thermodynamic database by Chen et al., the liquid phase was modeled as $(Y^{3+}, Zr^{4+})_p (O^{2-})_q$ in which $p = 2y_{O^{2-}}$ and $q = 3y_{Y^{3+}} + 4y_{Zr^{4+}}$ [13]. The Gibbs energy description of liquid is given by:

$$G^L_m = y_{Y^{3+}} y_{O^{2-}} \, {}^\circ G^L_{Y^{3+}:O^{2-}} + y_{Zr^{4+}} y_{O^{2-}} \, {}^\circ G^L_{Zr^{4+}:O^{2-}} + pRT[y_{Y^{3+}} \ln y_{Y^{3+}} + y_{Zr^{4+}} \ln y_{Zr^{4+}}] + {}^E G^L_m$$

The excess Gibbs energy ${}^E G^L_m$ is defined as below:

$$^E G^L_m = y_{Y^{3+}} y_{Zr^{4+}} y_{O^{2-}} \sum_{i=0}^{n} {}^i L_{Y^{3+}, Zr^{4+}:O^{2-}} (y_{Y^{3+}} - y_{Zr^{4+}})^i$$

The ionic liquid was considered as sub-sub-regular solution (i=2) in the database by Chen et al. [13].

Generally, the liquid phase is stable at high temperatures. In order to model an amorphous phase in the CALPHAD approach, one method is to extrapolate the liquid model to lower temperatures. In fact, the amorphous phase is considered as a supercooling liquid. Although the structure and physical state of supercooling liquid is different from amorphous phase and some minor errors are expected in this simulation, but they are still very similar and the results are close to reality.

### 3.4. *Gibbs energy calculation for nano particles:*

The surface area becomes significant and plays an effective role in the Gibbs energy in nano particles. Consequently, the Gibbs energy equation will be as shown below for nano particles:

$$\Delta G_{total} = \Delta G_{bulk} + \gamma A = \Delta H_{bulk} - T\Delta S_{bulk} + \gamma A \qquad (2)$$

in which $\gamma$ is specific surface energy and A is surface area of the nano particles. Therefore, in order to calculate the total Gibbs energy for nano particles, specific surface energy of each phase and the surface area are needed. The experimental data for the specific surface energy of n-YSZ polymorphs provided by Drazin and Castro [17] at room temperature were applied in this study to calculate surface energy. The particles were also assumed to be spherical to enhance surface area calculation.

### 4. *Results and discussion:*

Figure 3 shows the calculated Gibbs energy of bulk YSZ vs. composition (mole fraction of $Y_2O_3$) for the four phases i.e. monoclinic, tetragonal, cubic, and amorphous (supercooling liquid), at room temperature. The yttria mole fraction is between 0 and 0.2 since the zirconia rich side has important applications as mentioned in section 1.
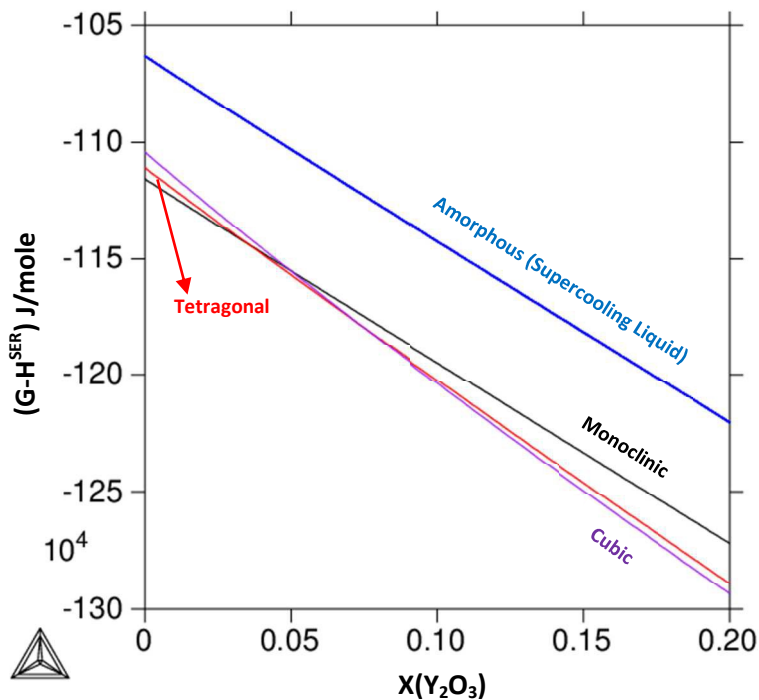
*Figure 3- The Gibbs energy of monoclinic, tetragonal, cubic, and amorphous (supercooling liquid) phases vs. yttria mole fraction at room temperature for the bulk YSZ.*

Based on the experimental results followed by statistical analyses, the equations below from Drazin and Castro represent the specific surface energy of each n-YSZ polymorph [17]:

$$\gamma_m = (1.9278)-(9.68)x \tag{3}$$

$$\gamma_t = (1.565)-(4.61)x \tag{4}$$

$$\gamma_c = (1.1756)-(3.36)x+(7.77)x^2 \tag{5}$$

$$\gamma_a = (0.8174)-(0.11)x \tag{6}$$

In all these equations, x is the yttria mole fraction and $\gamma_m$, $\gamma_t$, $\gamma_c$, and $\gamma_a$ are specific surface energies of monoclinic, tetragonal, cubic, and amorphous phases respectively.

For solids, the specific surface energy depends on the particle size ($d\gamma/dA \neq 0$) [21] in addition to the composition. However, for the particles with radii greater than the critical radius ($R \geq R_c$), the specific surface energy is constant at a determined temperature and does not change with particle size [22]. Based on the results of

previous studies on the molecular systems, $R_c$ is between 0.5 and 1 nm [22], which is less than almost the whole particle size range studied in the current paper. Therefore, the specific surface energies are dependent only on the yttria mole fraction in this study as it is indicated in the equations 3, 4, 5, and 6.

The total Gibbs energy of n-YSZ system is predicted as shown in Figure 4 for particle size (the spherical particle diameter) of 0.1 nm, 1 nm, 10 nm, and 100 nm at room temperature.
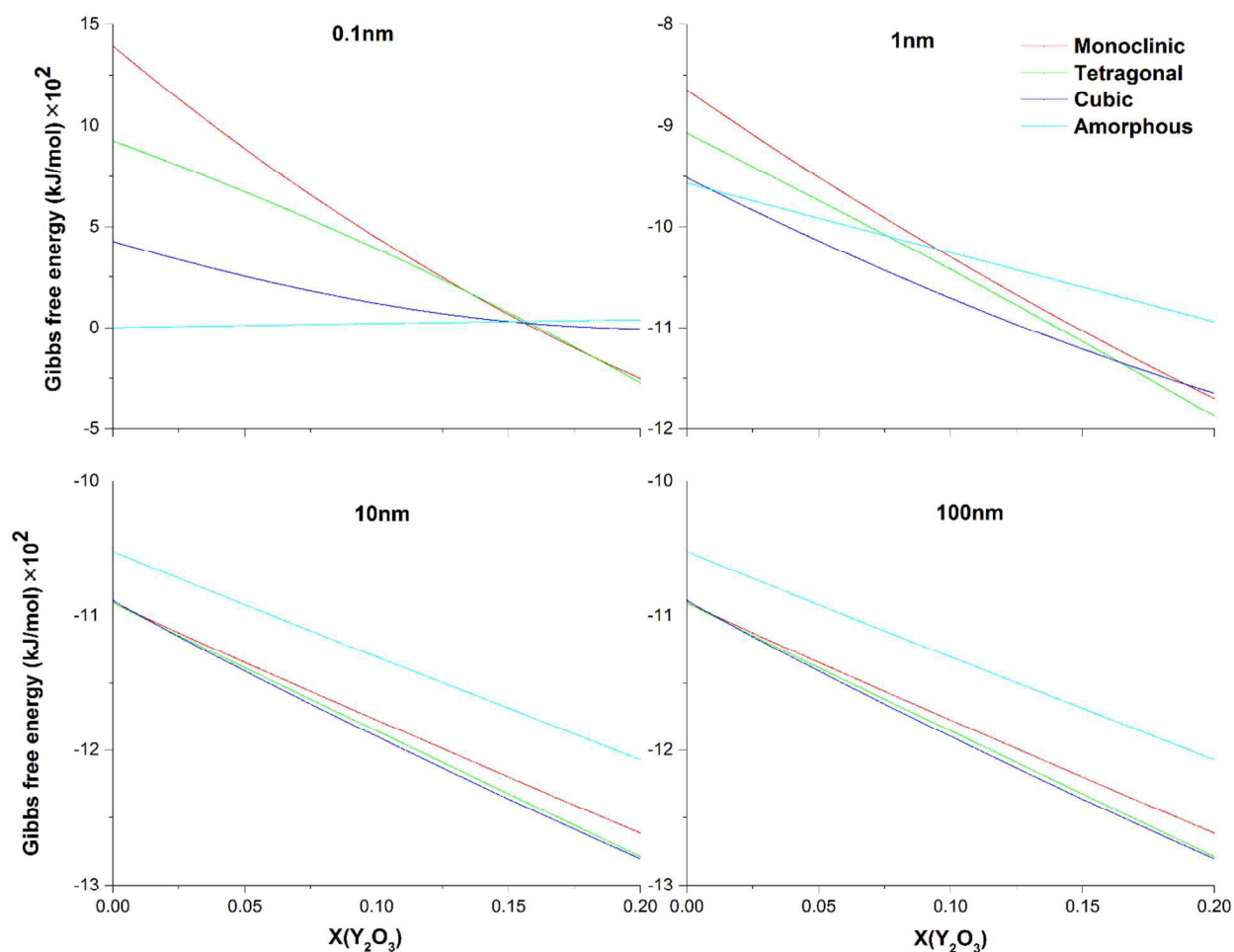


*Figure 4- The Gibbs energy vs. yttria mole fraction at room temperature for n-YSZ with different particle sizes.*

As it is shown in Figure 4, the intersection between Gibbs energy of different phases is changing with particle size. When the particle size is 10 or 100 nm, amorphous phase is not stable. If the particle size decreases to 1 nm, the amorphous phase starts to be stable

and its stability composition range increases by decreasing the particle size (Figure 4). As the stability of each phase is determined by the Gibbs energy of that phase, for a specific phase to be stable, its Gibbs energy needs to be less than that of the other involved phases. The Gibbs energy of amorphous phase is less than cubic, tetragonal, and monoclinic phases only when the size of particles are very small. When the particle size decreases, the effect of surface energy increases which causes the Gibbs energy of all involved phases to be changed and leads to stability of amorphous phase rather than cubic, tetragonal and monoclinic phases.

The intersection points indicate that the Gibbs energies of the two phases related to each intersecting curve are equal at a certain composition. These intersection points for each two adjacent phases represent $T_0$ temperature line which was discussed in section 3.2. Using T-zero method, n-YSZ phase diagram at room temperature was plotted as indicated in Figure 5. In this figure, each curve indicates the boundary between phases by which the stability range of each polymorph vs. particle size and composition (mole fraction of $Y_2O_3$) is detected at room temperature. The Y axis in Figure 5 is in logarithmic scale.
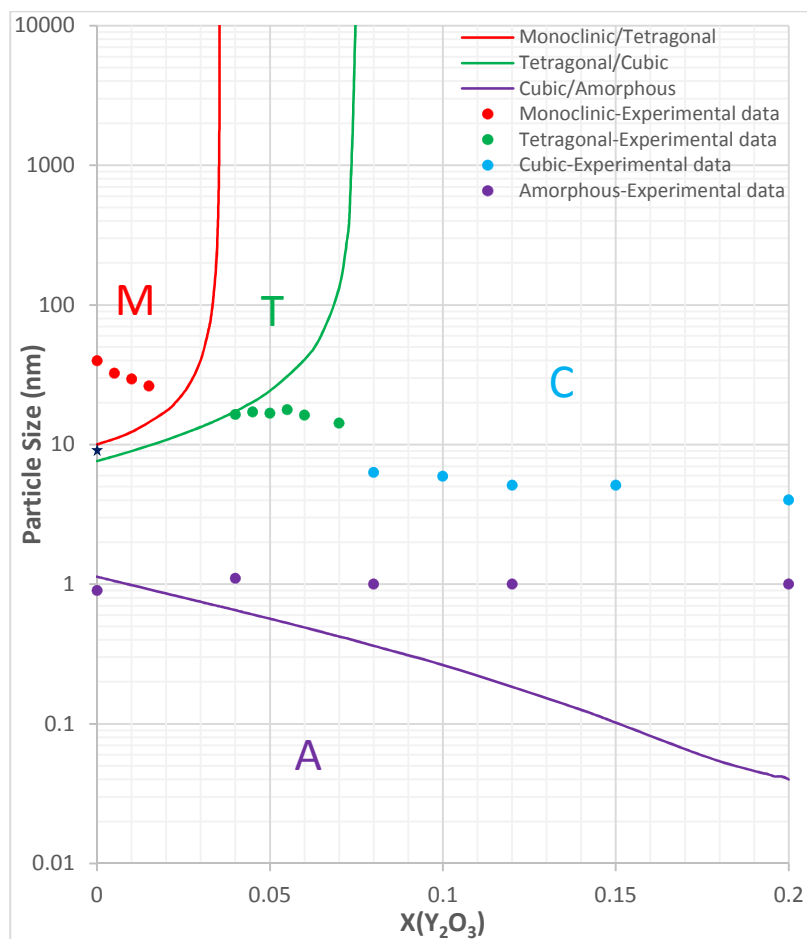
*Figure 5- The phase diagram for n-YSZ system at room temperature in comparison with the experimental data which represent experimentally measured crystal structure by Drazin and Castro [17]. ★sign indicates the largest tetragonal pure zirconia particle size experimentally observed [17]. (M: Monoclinic, T: Tetragonal, C: Cubic, A: Amorphous)*

The largest tetragonal pure zirconia particle size experimentally observed was around 9 nm [17] which is compatible with the diagram in Figure 5. Due to simplifications as discussed in section 3.3, the errors are expected for the amorphous phase in the current study. However, the results for amorphous phase clearly indicate the ability of predicting the amorphous stability range by the CALPHAD approach along with its critical role to predict the Gibbs energy of other phases. The discrepancy between tetragonal phase region and the related superimposed experimental data shown in Figure 5 can be an indication that the thermodynamic database for bulk YSZ provided by Chen et al. [13] needs to be improved in tetragonal+cubic/cubic phase boundary. It is found there were no experimental data for the T′o line shown in Figure 7 at the time of thermodynamic database assessment, while enough experimental data were available

for $T_0$ temperature line [13]. Then, it is highly possible that the $T'_0$ line is not accurate and needs to be shifted toward right side of the graph which will then provide better agreement between tetragonal/cubic (T/C) curve and related experimental data.

It is worth noting that in Figure 5, the role of bulk Gibbs energy is of great importance. The phase stability regions will greatly change if the bulk Gibbs energy is not calculated correctly. For example, the $\Delta H_{M/T}$ and $\Delta H_{T/C}$ calculated with oxide melt drop solution calorimetry method by Drazin and Castro are 10.304 and 13.351 (kJ/mol) respectively [17], while $\Delta H_{M/T}$ and $\Delta H_{T/C}$ is 6 and 7.5 (kJ/mol) respectively based on the thermodynamic database from Chen et al. by the CALPHAD approach [13]. It is highly possible these large differences are due to the stability state of the samples which experimentally investigated. If the examining sample does not reach the final equilibrium, which is highly possible in YSZ system due to its extremely slow kinetics, the measured enthalpy of this sample will be different with that of the same sample in its final equilibrium state.

Since the CALPHAD approach was applied in this study, the Gibbs energy of bulk YSZ is predictable in a wide range of temperature. Therefore, the Gibbs energy of bulk YSZ for each phase was predicted with the CALPHAD approach at different temperatures between 25 to 500°C. By considering the effect of surface energy, the n-YSZ phase diagram at various temperatures is predicted as shown in Figure 6. The specific surface energy of a crystal structure depends on the temperature [23]. Accordingly, the specific surface energy at a determined particle size and composition will change with temperature. In this study, the changes of specific surface energy by increasing the temperature up to 500°C was assumed to be small and negligible.

Comparing the four diagrams in Figure 6, the $c$-$ZrO_2$ region is enlarged with the increase of temperature. The stability range of $m$-$ZrO_2$ shrinks and the T/C curve shifts toward left side of the graph and also moves up when temperature increases. The changes in stability range of phases with temperature clearly show how the crystal structure and as a result, material properties change. For example, based on Figure 6, a 10n-0.01YSZ system (YSZ with yttria mole fraction of 0.01 and particle size of 10 nm) is tetragonal at room temperature which changes to cubic at temperatures around 500°C.

This phase transition can affect the material properties which is directly linked to the crystal structure.

One may argue that a phase diagram for nano particles at high temperatures is not applicable because nano particles will encounter coarsening at high temperatures. However, the phase diagram for nano particles can clearly reveal the effect of temperature increase and coarsening on the phase transition.

Interestingly according to Figure 6, the cubic/amorphous (C/A) curve is predicted not to change considerably by increasing temperature. This prediction is due to the effect of surface energy which is greatly dominant rather than the bulk Gibbs energy since the particle size in the amorphous region is extremely small (Eq. 2). Since the specific surface energy was assumed to be constant with temperature changes, the surface energy does not change with temperature and this causes the C/A curve be approximately fixed with temperature changes.
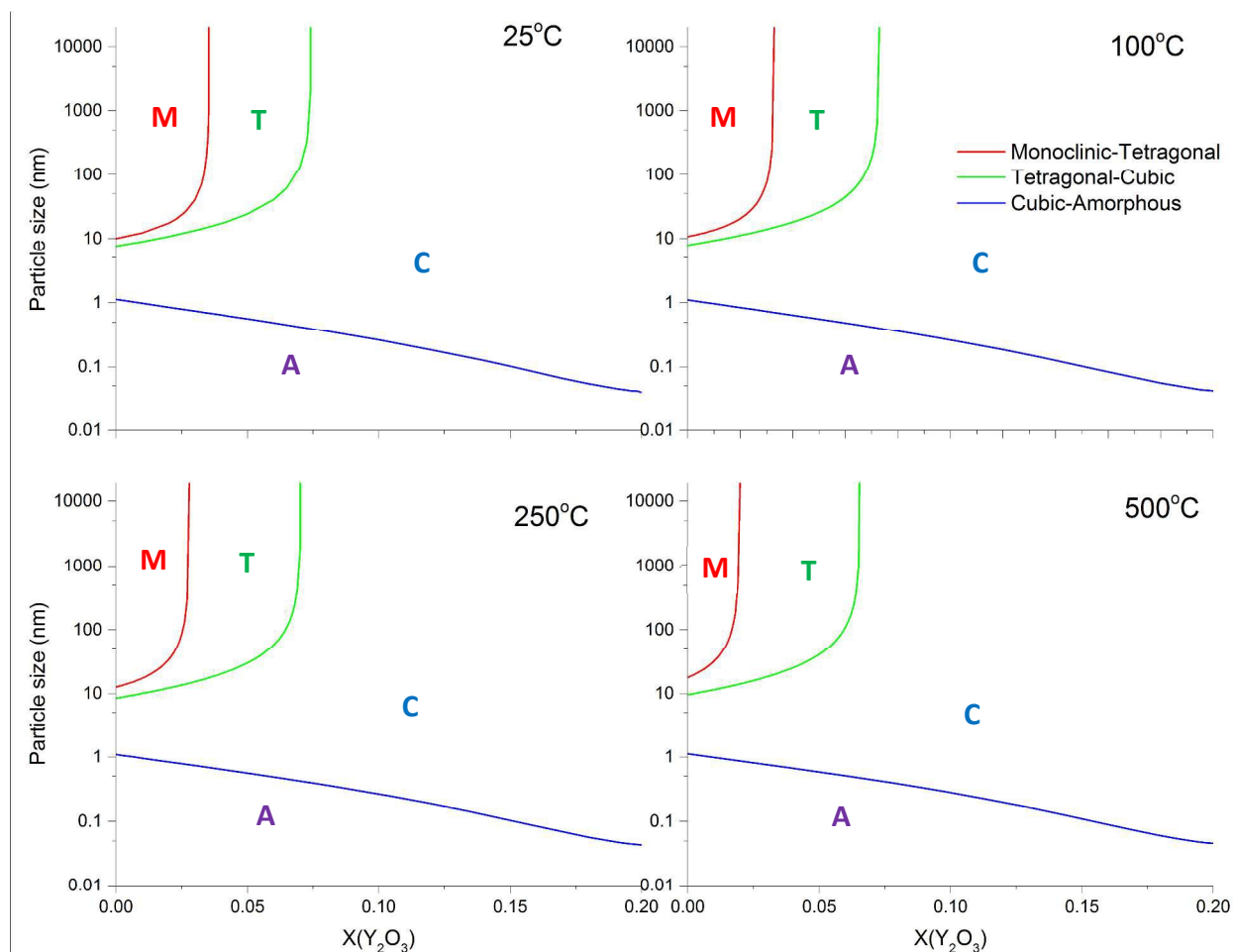


Figure 6- The phase diagram for n-YSZ system at 25, 100, 250, and 500°C. (M: Monoclinic, T: Tetragonal, C: Cubic, A: Amorphous)

12

The shift of T/C curve vs. temperature is less than that of monoclinic/tetragonal (M/T) curve as can be seen in Figure 6. According to Figure 7, in the temperature range of 25 to 500°C, the slope of T´$_0$ line is sharper than that of T$_0$ temperature line. This slope difference is the reason for milder shift of T/C curve rather than M/T curve vs. temperature changes. As an example of the shifting amount of each curve vs. temperature, Figure 8 shows the shifting behavior of M/T, T/C, and C/A curves when temperature increases for n-0. 01YSZ.
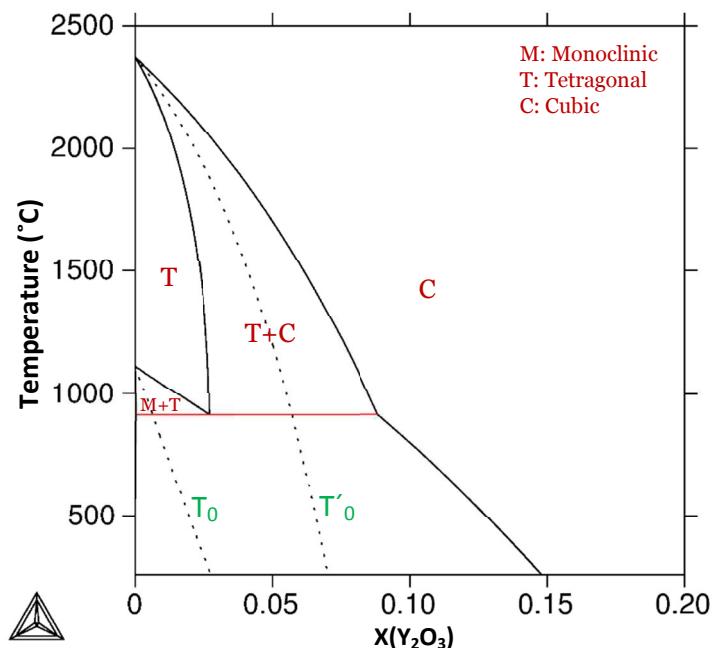


*Figure 7- T$_0$ and T´$_0$ temperature lines related to bulk YSZ. (T$_0$ is M/T T-zero temperature line and T´$_0$ is T/C T-zero temperature line).*
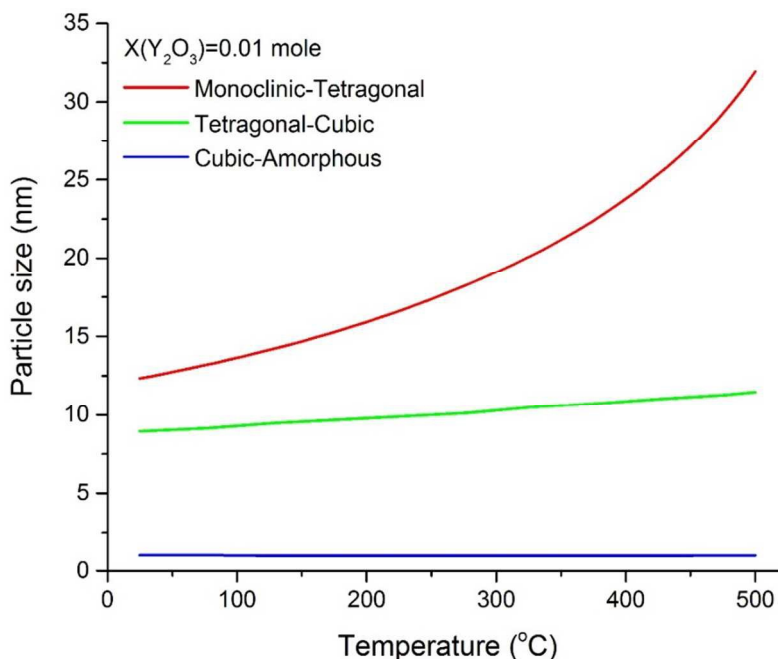
*Figure 8- The changes of particle size vs. temperature for each boundary curve of n-0. 01YSZ (Nano YSZ with 0. 01 mole fraction of Y₂O₃).*

By combining the phase diagrams at different temperatures, a 3-D phase diagram was achieved in which the phase regions are predicted based on the particle size, mole fraction of yttria and temperature. Figure 9 indicates the 3-D phase diagram for n-YSZ system from different angles.
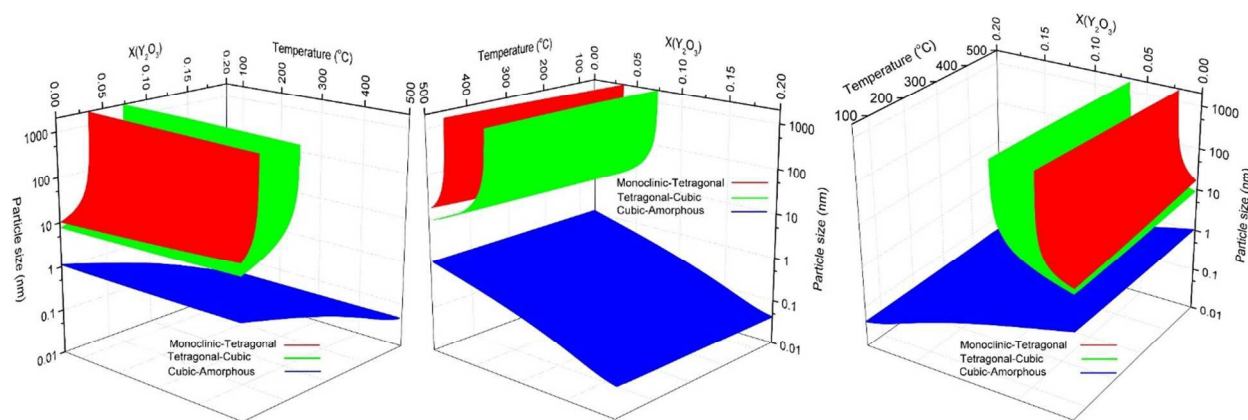


*Figure 9- The 3-D phase diagram for n-YSZ system from different angles.*

## 5. *Conclusion:*

The phase diagram for n-YSZ system at room temperature was developed with the bulk Gibbs energies from the CALPHAD approach and specific surface energies of each crystal structure. By the advantage of the CALPHAD approach characteristics, the total Gibbs energy of n-YSZ system at higher temperatures was predicted and the 3-D diagram for zirconia rich side was developed at temperatures up to 500°C for the first time, by which the stability range of each phase in n-YSZ system is predicted based on particle size, composition, and temperature. Based on the 3-D diagram, the $c$-$ZrO_2$ and $t$-$ZrO_2$ regions become more stable and wider when temperature increases while the $m$-$ZrO_2$ region shrinks. It was shown that the CALPHAD approach plays a pivotal role to design a predictive phase diagram for nano particles. It was indicated that the CALPHAD approach is capable to be used for predicting the Gibbs energy of amorphous phases by considering few assumptions.

References:

[1]    C. H. Wang, M. C. Wang, J. K. Du, Y. Y. Sie, C. S. Hsi, and H. E. Lee, "Phase transformation and nanocrystallite growth behavior of 2 mol% yttria-partially stabilized zirconia (2Y-PSZ) powders," *Ceram. Int.*, vol. 39, no. 5, pp. 5165–5174, 2013.

[2]    J. Chevalier, L. Gremillard, A. V. Virkar, and D. R. Clarke, "The tetragonal-monoclinic transformation in zirconia: Lessons learned and future trends," *J. Am. Ceram. Soc.*, vol. 92, no. 9, pp. 1901–1920, 2009.

[3]    J. R. Kelly and I. Denry, "Stabilized zirconia as a structural ceramic: An overview," *Dent. Mater.*, vol. 24, no. 3, pp. 289–298, 2008.

RSC Advances Accepted Manuscript

[4]     A. Nakamura and J. B. Wagner, "Defect structure, ionic conductivity, and diffusion in yttria stabilized zirconia and related oxide electrolytes with fluorite structure," *J. Electrochem. Soc.*, vol. 133, no. 8, pp. 1542–1548, 1986.

[5]     W. Strickler and W. G. Carlson, "Ionic Conductivity of Cubic Solid Solutions in the System CaO-Y2O3-ZrO2," *J. Am. Ceram. Soc.*, vol. 47, no. 3, pp. 122–127, 1963.

[6]     Y. Li, Z. Tang, Z. Zhang, and J. Gong, "Electrical conductivity of zirconia stabilized with yttria and calcia," *J. Mater. Sci. Lett.*, vol. 18, no. 6, pp. 443–444, 1999.

[7]     A. Cirera, C. Lpez-Gándara, and F. M. Ramos, "YSZ-based oxygen sensors and the use of nanomaterials: A review from classical models to current trends," *J. Sensors*, vol. 2009, 2009.

[8]     R. H. R. Castro, "On the thermodynamic stability of nanocrystalline ceramics," *Mater. Lett.*, vol. 96, pp. 45–56, 2013.

[9]     R. Garvie, "The occurrence of metastable tetragonal zirconia as a crystallite size effect," *J. Phys. Chem.*, vol. 147, no. 1950, pp. 1238–1243, 1965.

[10]   R. Garvie and P. Nicholson, "Phase analysis in zirconia systems," *J. Am. Ceram. Soc.*, no. June, pp. 303–305, 1972.

[11]   N. S. Jacobson, L. Kaufman, F. Zhang, and C. Llc, "Thermodynamic Modeling of the YO1.5-ZrO2 System," *J. Am. Ceram. Soc.*, vol. 1566, pp. 1559–1566, 2004.

[12]   Y. Du, Z. Jin, and P. Huang, "Thermodynamic Assessment of the Zr01-Y01.5 System," *J. Am. Ceram. Soc.*, vol. 74, no. 7, pp. 1569–1577, 1991.

[13]   M. Chen, B. Hallstedt, and L. J. Gauckler, "Thermodynamic modeling of the ZrO2-YO1.5 system," *Solid State Ionics*, vol. 170, no. 3–4, pp. 255–274, 2004.

[14]   H. Ding, A. V. Virkar, and F. Liu, "Defect configuration and phase stability of cubic versus tetragonal yttria-stabilized zirconia," *Solid State Ionics*, vol. 215, pp. 16–23, 2012.

[15]   A. Suresh, M. J. Mayo, and W. D. Porter, "Thermodynamics For Nanosystems: Grain And Particle-Size Dependent Phase Diagrams.," *Rev. Adv. Mater. Sci.*, vol. 5, no. 2, pp. 100–109, 2003.

[16]　J. a. Krogstad, M. Lepple, Y. Gao, D. M. Lipkin, and C. G. Levi, "Effect of yttria content on the zirconia unit cell parameters," *J. Am. Ceram. Soc.*, vol. 94, no. 12, pp. 4548–4555, 2011.

[17]　J. W. Drazin and R. H. R. Castro, "Phase Stability in Nanocrystals: A Predictive Diagram for Yttria-Zirconia," *J. Am. Ceram. Soc.*, vol. 1384, pp. 1377–1384, 2015.

[18]　J. W. Drazin and R. H. R. Castro, "Water adsorption microcalorimetry model: Deciphering surface energies and water chemical potentials of nanocrystalline oxides," *J. Phys. Chem. C*, vol. 118, no. 19, pp. 10131–10142, 2014.

[19]　B. Jansson, "Trita-Mac-0234," *R. Inst. Technol. Stock. Sweden*, 1984.

[20]　L. Kaufman and M. Cohen, "Thermodynamics and kinetics of martensitic transformations," *Prog. Met. Phys.*, vol. 7, pp. 165–246, 1958.

[21]　D. A. Porter, K. E. Easterling, and M. Sherif, *Phase Transformations in Metals and Alloys, (Revised Reprint)*. CRC press, 2009.

[22]　V. M. Samsonov,  a. N. Bazulev, and N. Y. Sdobnyakov, "On applicability of Gibbs thermodynamics to nanoparticles," *Cent. Eur. J. Phys.*, vol. 1, no. 3, pp. 474–484, 2003.

[23]　T. Frolov and Y. Mishin, "Temperature dependence of the surface free energy and surface stress: An atomistic calculation for Cu(110)," *Phys. Rev. B*, vol. 79, no. 4, pp. 1–10, 2009.